GA–A26728

# FIRST RESULTS EXAMINING THE COMPATIBILITY OF RMP ELM SUPPRESSION WITH THE RADIATING DIVERTOR IN DIII-D

by

T.W. PETRIE, T.E. EVANS, M.E. FENSTERMACHER, S. MORDIJCK,
N.H. BROOKS, J.R. FERRON, B. HUDSON, A.W. HYATT, C.J. LASNIER,
A.W. LEONARD, T.C. LUCE, R.A. MOYER, P.A. POLITZER,
M.J. SCHAFFER, P.B. SNYDER, and J.G. WATKINS

JULY 2010

GENERAL ATOMICS

## DISCLAIMER

GA–A26728

# FIRST RESULTS EXAMINING THE COMPATIBILITY OF RMP ELM SUPPRESSION WITH THE RADIATING DIVERTOR IN DIII-D

by

**T.W. PETRIE, T.E. EVANS, M.E. FENSTERMACHER,* S. MORDIJCK,† N.H. BROOKS, J.R. FERRON, B. HUDSON,‡ A.W. HYATT, C.J. LASNIER,* A.W. LEONARD, T.C. LUCE, R.A. MOYER,† P.A. POLITZER, M.J. SCHAFFER, P.B. SNYDER, and J.G. WATKINS¶**

This is a preprint of a paper to be presented at the Nineteenth International Conference on Plasma Surface Interactions, May 24-28, 2010, in San Diego, California, and to be published in the *J. Nucl. Mater.*

*Lawrence Livermore National Laboratory, Livermore, California.
†University of California-San Diego, La Jolla, California.
‡Oak Ridge Institute for Science Education, Oak Ridge, Tennessee.
¶Sandia National Laboratories, Albuquerque, New Mexico.

Work supported in part by
the U.S. Department of Energy
under DE-FC02-04ER54698, DE-AC52-07NA27344, DE-FG02-07ER54917, DE-AC05-06OR23100, DE-AC04-94AL85000, and DE-FG02-05ER54809

GENERAL ATOMICS ATOMICS PROJECT 30200
JULY 2010

GENERAL ATOMICS

## ABSTRACT

We report on recent DIII-D experiments that integrate edge localized mode (ELM) suppression using resonant magnetic perturbations (RMPs) with divertor heat flux reduction under radiating divertor conditions. Our results illustrate the limitations in maintaining ELM suppression at gas puffing levels that were representative of good puff and pump operation in previous experiments without RMP. The electron pressure gradient in the pedestal $(\nabla Pe)$ increased steadily during gas puffing and ELMs returned once $\nabla Pe$ reached values consistent with the peeling-ballooning stability limit, as determined by edge stability analysis. Even with this return of ELMs, a radiating divertor with RMP generated higher levels of total radiated power (~40%) than comparable standard ELMing discharges without RMP at the same density. Differences in the accumulation of the seed argon in the core plasma between RMP and non-RMP during puff and pump were less than 20%.

# I. INTRODUCTION

The transient heat loads to the wall material at the divertor targets during ELMs may result in severe erosion that may significantly shorten the lifetime of future, highly powered tokamaks [1]. Recent investigations, however, have demonstrated that such damaging ELMs can be mitigated or even suppressed by applying resonant magnetic perturbations (RMPs) to the pedestal region of the plasma [2-4]. While studies to improve understanding of the underlying physics are ongoing, the use of RMPs introduces a plausible option in mitigating or suppressing ELM-damage to divertor surfaces.

Despite the fact that RMPs effectively eliminate *transient* heat damage from ELMs, the *steady* heating component at the divertor targets for proposed highly powered tokamaks of the future, like ARIES-RS [5], might still be unacceptably high. In previous studies, radiating divertor solutions were effective in reducing and controlling the steady flow of heat to the divertor targets [6-9]. In DIII-D, the “puff and pump” scenario was found to be effective in reducing the overall power load at the divertor targets by increasing the power loss by radiation with little degradation of H-mode plasma properties. In the puff and pump approach, “seed” impurities are injected into the private flux region (PFR) and restrained from penetrating the plasma core by a combination of deuterium gas injection upstream and active particle exhaust at the divertor targets.

Separately, the RMP technique addresses the impulsive heat load from the ELMs and puff and pump addresses the steady heat load. It is unclear, however, whether RMP ELM suppression can be successfully merged with a radiating divertor solution. In this paper we examine this compatibility issue, particularly from the standpoints (1) of maintaining ELM suppression during gas injection and (2) of evaluating radiating divertor behavior with RMP. The experimental arrangement and methodology are described in Sec. II. In Sec. III we present our results and we discuss them in Sec. IV.

## II. EXPERIMENTAL SETUP

The poloidal cross-section of the unperturbed MHD equilibrium for the lower single-null (SN) used in this study is shown in Fig. 1. In-vessel, active pumping of the injected deuterium $(D_2)$ and argon (Ar) gases is done by a single cryo-pump located in the lower divertor plenum. The outer divertor strike point radius (Rosp) is situated adjacent to the entrance of the lower divertor plenum for maximum pumping. Argon is injected directly into the PFR, while $D_2$ is injected into the crown of the lower SN configuration in order to increase the deuterium ion flow toward the lower divertor pump. Argon is used as the seeded impurity in this experiment because it radiates effectively at the temperatures prevailing in both the divertor and pedestal regions of DIII-D H-mode plasmas and has a relatively short ionization mean free path. Carbon, generated by erosion of the graphite armor, is the dominant intrinsic impurity in DIII-D discharges. The plasmas in this study are characterized by: $I_P = 1.43$ MA, $B_T = 1.8$ T, $q_{95} = 3.5$, $P_{INJ} \approx 5.5$-$6.5$ MW, $H_{98(y,2)} \approx 0.9$-$1.2$, $\beta_N \approx 2$, $\bar{n}_e/n_{eG} \approx 0.3$-$0.7$, $P_{\mathrm{RAD}}/P_{\mathrm{INJ}} \approx 0.3$-$0.8$, $Z_{eff} \approx 2$, and the direction of the ion $\boldsymbol{B} \times \nabla B$ drift is toward the X-point.

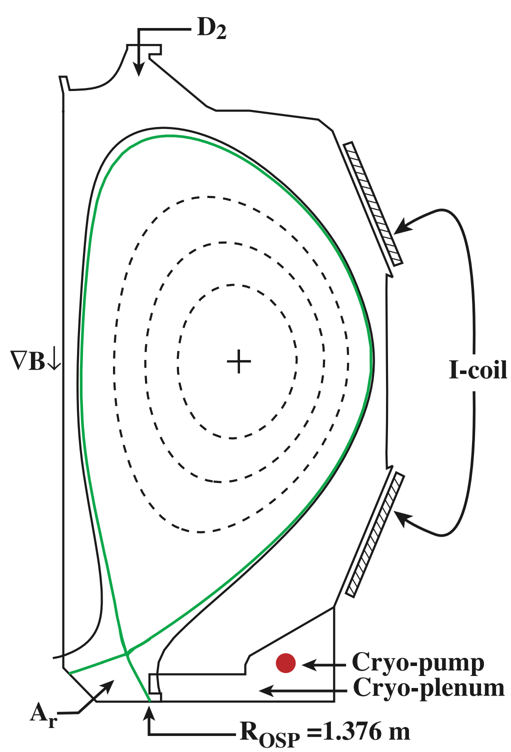


Fig. 1. Unperturbed MHD equilibrium cross-section of the lower single-null configuration with the gas injection, divertor pumping plenum, and RMP I-coil locations superimposed.

DIII-D has two off-axis rows of six internal coils each, the “I-coil”, that are used for ELM suppression and mitigation experiments in an $n = 3$ magnetic configuration [10]; the poloidal location of two of these coils is shown in Fig. 1. The experiments in this paper employed the I-coil with $n = 3$, $60°$ phasing in even parity. This means that the coils above and below the midplane at a given toroidal position are of the same polarity, i.e., up-down symmetric. For the maximum coil current, this results in a perturbation strength of $\delta b_r \sim 6.5 \times 10^{-4}$ T at $\Psi_N = 0.95$ [4]. The I-coil current used in this experiment was 5.8 kA, which at that time was slightly less than its maximum allowed value of 6.0 kA, and ELM suppression is obtained for an edge $q_{95}$ in the range 3.25-3.65.

# III. RESULTS

## A. ELM-suppression during gas puffing

Figure 2 shows that RMP-induced ELM suppression is diminished and ultimately lost even at modest rates of deuterium and argon injection [Figs. 2(IIa), 2(IIIa)]. The activation of the I-coils at $t = 2.0$ s results in an immediate decrease in the pedestal density $n_{\mathrm{PED}}$: $n_e/n_{e\mathrm{G}} = 0.5$ and 0.3 at $t = 1.9$ s (pre-activation of the I-coil) and 2.7 s (post-activation of the I-coil), respectively. The ELMs are suppressed within 200 ms of I-coil activation. Deuterium and argon injection begin at 2.8 s and 3.2 s, respectively. As with similar ELMing H-mode plasmas without RMP, higher $\Gamma_{\mathrm{D2}}$ produces a more rapid increase in $n_{PED}$ [Figs. 2(Ib)-2(IIIb)] and a measurable drop in pedestal electron temperature $T_{\mathrm{PED}}$ [Figs. 2(Ic)-2(IIIc)]. The energy confinement factor, $H_{98(y,2)}$, is 1.2 before the I-coil is activated, drops to $\approx 0.9$ following activation, and is constant for the rest of the discharge [Figs. 2(Id)-2(IIId)]. After the initial drop in the edge electron pressure gradient $\nabla P_e$ [Figs. 2(Ie)-2(IIIe)] following I-coil activation, $\nabla P_e$ partially recovers during subsequent gas puffing; $\nabla P_e$ is determined just prior to an ELMing event within the pedestal. The higher the deuterium gas puff rate, the sooner ELMs reappear. The range in $n_{\mathrm{PED}}$ for ELM-suppressed operation is relatively small for these puff and pump plasmas.

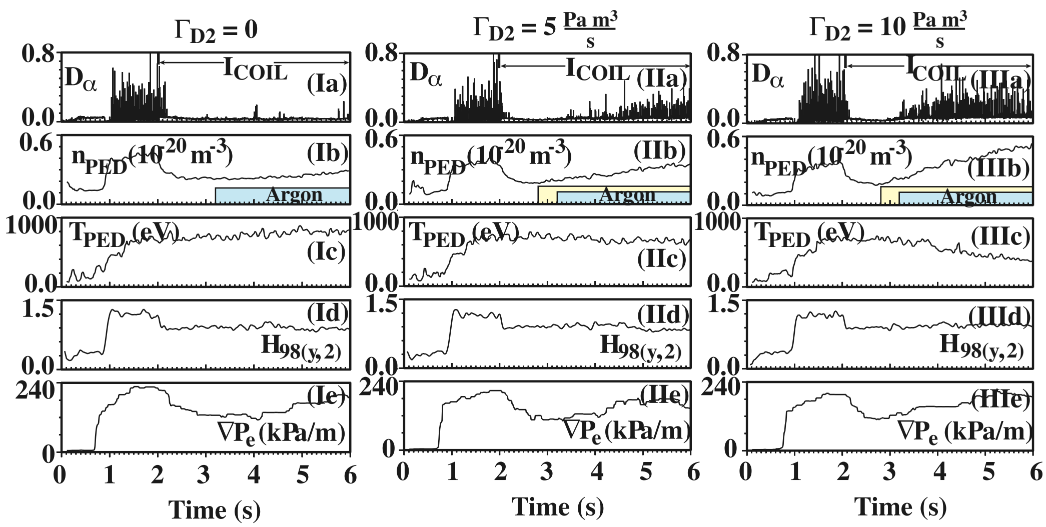


Fig. 2. The re-emergence of ELMing activity for three discrete values of $\Gamma_{\mathrm{D2}}$: 0, 5, and 10 Pa m$^3$/s in columns I, II, and III, respectively. (a) Deuterium recycling $D_\alpha$, (b) $n_{\mathrm{PED}}$, (c) $T_{\mathrm{PED}}$, (d) $H_{98(y,2)}$, and (e) $\nabla P_e$. Note that the argon (blue) and the deuterium (yellow) boxes in (b) represent only their injection times and are not to scale. $\Gamma_{\mathrm{Ar}} = 0.05$ Pa m$^3$/s and I-coil = 5.8 kA in each case.

In Fig. 3, the electron collisionality in the pedestal $\left(\nu_e^*\right)$ [11] and the maximum gradient in the pedestal electron pressure $\left(\nabla P_{e-\mathrm{MAX}}\right)$ are plotted versus $n_{\mathrm{PED}}$ for three phases of these H-mode discharges: (1) ELMing, (2) transition ELM behavior, and (3) ELM-suppressed (Fig. 3). While the ELMing and ELM-suppressed phases are self-explanatory, the *transitional* phase refers to times where sporadic ELMing is occurring. During the ELMing phase before the I-coil is activated, the average $n_{\mathrm{PED}}$ is $\approx 0.39\times10^{20}$ m$^{-3}$. Shortly after I-coil activation, ELM-suppression is observed when $n_{\mathrm{PED}}$ is in the range (0.17-0.25) $\times10^{20}$ m$^{-3}$, a *transition* interval for $n_{\mathrm{PED}} \approx$ (0.25-0.30) $\times10^{20}$ m$^{-3}$, and finally for $n_{\mathrm{PED}} > 0.30\times10^{20}$ m$^{-3}$, a return to the "pure" ELMing regime. Figure 3 shows that even for modest increases in the gradient of the pedestal pressure, ELM-suppressed plasmas can transition to solidly ELMing H-mode discharges. Analysis using the ELITE edge plasma stability code [12] suggests that peeling-ballooning mode instabilities trigger the onset of these type-1 ELMs. Hence, it is not surprising that an increase in pedestal $\nabla P_e$ may promote the re-emergence of ELMing.

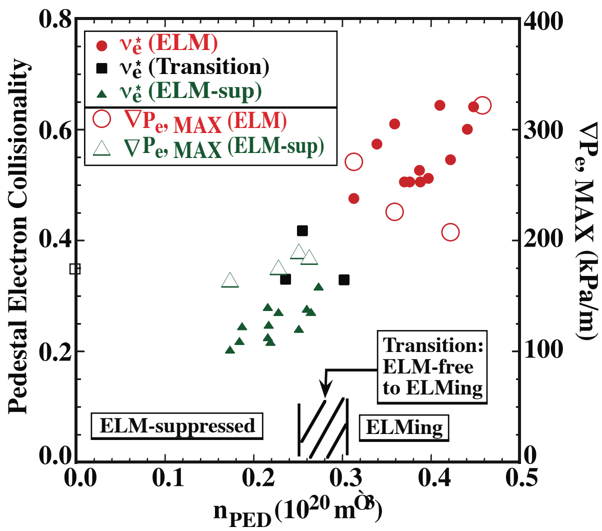


Fig. 3. Electron collisionality and the maximum pressure gradient in the pedestal are plotted versus $n_{\mathrm{PED}}$. $\Gamma_{\mathrm{D2}}$ = 0-10 Pa m$^3$/s and $\Gamma_{\mathrm{Ar}}$ = 0.05 Pa m$^3$/s.

While the reappearance of ELMing can be associated with increases in pedestal $\nabla P_e$, the precise role of pedestal electron collisionality in the reappearance of ELMing is less clear. Changes in $\nu_e^*$ due to fueling effects may alter the pedestal stability limits, as suggested in [11,13]. ELM-suppression is observed for plasmas with $\nu_e^* < 0.3$ (consistent with Ref. [8]), the transition from ELM-suppressed to ELMing with $\nu_e^* \approx$ 0.3-0.45, and the ELMing regime with $\nu_e^* > 0.45$.

## B. Argon accumulation in the main plasma

Differences in argon accumulation inside the main plasma between RMP and similar non-RMP ELMing H-mode plasmas were less than 20% [Fig. 4]. As with the non-RMP cases, the core concentration of argon in the RMP cases decreases with increasing $\Gamma_{D2}$ for a constant argon injection rate $\Gamma_{Ar} = 0.05$ Pa m$^3$/s This suggests that many of the physical processes detailed in UEDGE [14] fluid transport modeling reported previously for non-RMP radiating divertor plasmas [9] may also be important in these corresponding RMP cases, e.g., the importance of particle drifts in "fueling" the core plasma. This is a key point, because the extensive studies in optimizing performance of radiating divertor plasmas in *non-RMP* cases provide direction as to how radiating divertor cases *with RMP* might be optimized. The return of Type-1 ELMing activity at the higher gas puff rates (or higher $n_{PED}$) in RMP plasmas may be responsible for the similarity in argon impurity accumulation in the main plasma. UEDGE modeling of these RMP plasmas is underway.

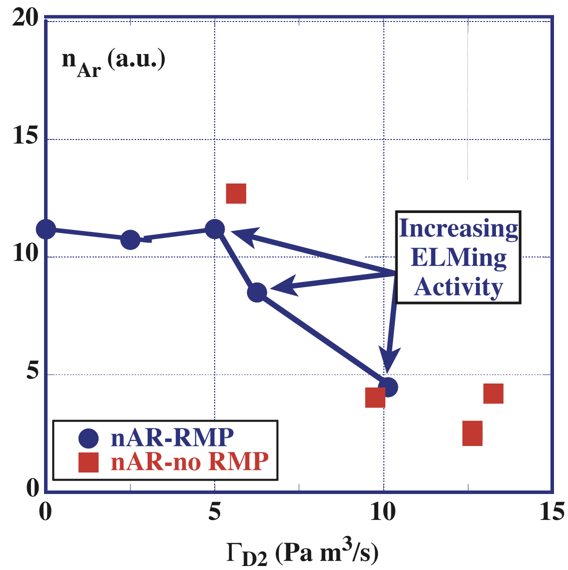


Fig. 4. Relative core argon accumulation in the core plasma $(n_{Ar})$ as a function of $\Gamma_{D2}$, in both RMP and non-RMP radiating divertor discharges. The methodology in determining $n_{Ar}$ is described in Ref. [15]. $\Gamma_{Ar} = 0.05$ Pa m$^3$/s in all cases.

## C. Radiating divertor with RMP

When RMP and puff and pump methods are applied together, there is a significant increase in radiated power over standard ELMing H-mode plasmas *at the same pedestal density*. A comparison of similarly prepared H-mode plasmas with and without RMP (but with the same $n_{PED}$) shows that the ratio of radiated power to input power $(P_{RAD}/P_{IN})$ was $\approx 40\%$ higher in the RMP puff and pump case than for the corresponding standard ELMing H-mode case (Fig. 5). Approximately one-third of this increase occurred in the

SOL and divertor regions and two-thirds of this increase in the main plasma. The increase in the SOL and divertor radiated power was largely due to the higher puffing rates of deuterium (and argon "seed" impurity) required to maintain the pedestal density (i.e., $n_{PED} \approx 0.39 \times 10^{20}$ m$^{-3}$) after the I-coil is activated. In turn, this produced a higher SOL density and lower plasma temperatures in both the plasma edge and SOL/divertor that favored higher radiated power. The increase in the radiated power in the main plasma was largely due to the accumulation of argon and a 10-15% reduction in $T_{PED}$. While $H_{98(y,2)}$ was reduced $\approx$ 25% after the I-coil was activated, the energy confinement time during subsequent deuterium and argon puffing continued to be representative of a good H-mode [i.e., $H_{98(y,2)} \approx 0.9$] and was insensitive to changes in $n_{PED}$. While ELMing re-appeared during the gas puffing phases with higher $\Gamma_{D2}$, we found that the *peak heat flux* deposited at the inner divertor targets during an ELM event was $\approx$ 30-40% lower than its pre-coil levels for the cases $n_{PED} \approx 0.39 \times 10^{20}$ m$^{-3}$, and $\approx$ 60-70% lower when $n_{PED} \approx 0.50 \times 10^{20}$ m$^{-3}$.

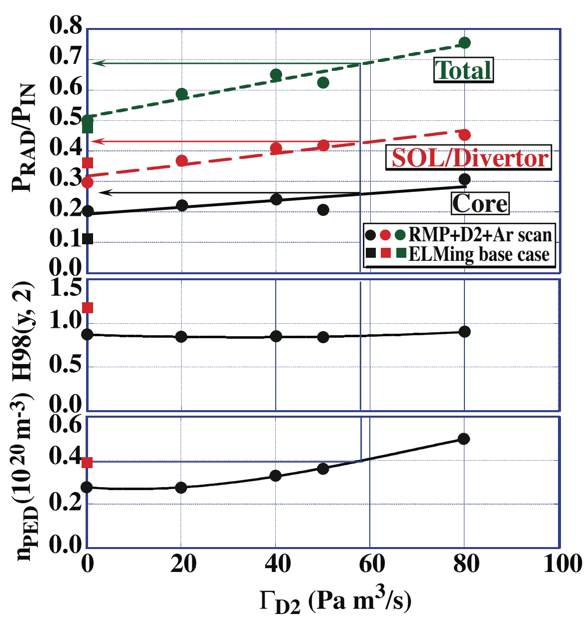


Fig. 5. (a) $P_{RAD}/P_{IN}$, (b) $H_{98(y,2)}$, and (c) $n_{PED}$ are plotted versus $\Gamma_{D2}$. $\Gamma_{Ar}$ is fixed at 0.05 Pa m$^3$/s. Data with RMP are shown for a range in $\Gamma_{D2}$ (solid circle). The reference case of ELMing without RMP is shown for $\Gamma_{D2} = 0$ (solid box). Plasma parameters: $I_p$ = 1.43 MA, $q_{95}$ = 3.5, and $P_{IN}$ = 5.4–6.5 MW.

## IV. DISCUSSION

ELMing activity in these plasmas ceased shortly after the activation of the I-coil, and both $n_{\mathrm{PED}}$ and $\nabla P_e$ in the pedestal were reduced $\approx 50\%$. When deuterium and argon gas were injected, both $n_{\mathrm{PED}}$ and $\nabla P_e$ at the edge increased. However, when ELMing re-emerged, $n_{\mathrm{PED}}$ had only recovered to $\approx 70\%$ and $\nabla P_e$ only $\approx 80\%$ of their pre-activation values. Because ELITE code analysis suggests that peeling-ballooning mode instabilities may be triggering the re-appearance of ELMs, the observed increases in $\nabla P_e$ during "recovery" may be associated with making the pedestal more susceptible to ELMs. Figure 3 suggests that the "headroom" in pedestal $\nabla P_e$ between ELM-suppressed and the ELMing conditions is relatively small for the plasmas under investigation.

Successful ELM suppression by RMP clearly puts a limit on $\Gamma_{\mathrm{D2}}$ (and $\Gamma_{\mathrm{Ar}}$) that is available for the puff and pump operation. Previous studies of the puff and pump approach at DIII-D have shown that higher $\Gamma_{\mathrm{D2}}$ leads to better screening of the seed impurity from the main plasma [8]. The "best" puff and pump results for the plasmas described here would require $\Gamma_{\mathrm{D2}} \sim 12\text{-}13$ Pa m$^3$/s, which is considerably above the maximum allowed $\Gamma_{\mathrm{D2}}$ for complete ELM-suppression (i.e. $< 3.5$ Pa m$^3$/s). These results highlight the challenges for future devices in combining RMP-based ELM suppression with optimal puff and pump radiating divertor.

Two ways that might extend the range in ELM-suppression are worth considering. The first approach focuses on inhibiting the buildup of pedestal $\nabla P_e$, since our results suggest that the increase in pedestal $\nabla P_e$ enhances the chance of triggering an ELM. Two possibilities to consider here are (1) increasing the I-coil current during gas puffing and (2) directing ECH absorption in the pedestal. In the former, sufficient power supplies for the I-coil is the crucial consideration, although increases in I-coil current that would degrade energy confinement and plasma performance is another downside. In the latter, ECH applied to plasma edge may enhance particle transport near the maximum in $\nabla P_e$ and thus inhibit the building of $\nabla P_e$.

The second general approach is based on enhancing the particle exhaust by exploiting what we learned in previous puff and pump experiments about how particle drifts affect pumping effectiveness. In the plasma discussed here, particle pumping was done only on the outer divertor leg with the ion $\boldsymbol{B} \times \nabla B$ drift directed toward the X-point. While this arrangement has been successful in suppressing ELMs, compared with the other pumping configurations available on DIII-D, this arrangement is least effective in controlling particle inventory and fueling of the main plasma, and hence in maintaining the lower density (and collisionality) conditions favorable to ELM suppression. Based on previous work in non-RMP radiating divertors [9], we postulate that the most effective way to control particle inventory (and preserve RMP ELM suppression) is to maximize the divertor pumping and to operate with the ion $\boldsymbol{B} \times \nabla B$ drift directed away from the X-point. For DIII-D, this would mean SN operation in the closed upper divertor which has much stronger pumping, i.e., two cryo-pumps available, with the ion $\boldsymbol{B} \times \nabla B$ drift directed away from the X-point. A discussion of the technical issues that we encountered in executing these ideas (e.g., avoiding 2/1 locked modes at low density) will be explored in a future paper.

While primary interest in RMP has been largely directed toward ELM-suppression, we found that the puff and pump radiating divertor, augmented with RMP, yielded significantly higher radiative fractions than the standard ELMing H-mode plasma at the same $n_{\mathrm{PED}}$. At a slightly higher pedestal density (i.e., $n_{\mathrm{PED}} \approx 0.50 \times 10^{20}$ m$^{-3}$), the fraction of radiated power increased further to 0.75. The energy confinement factor $H_{98(y,2)}$ was insensitive to the higher gas puff rate that this required. Even though ELMs re-appeared during the gas puffing phase for several cases discussed in Sec. III*C*, we found that the *peak heat flux* deposited at the inner divertor targets during an ELM event could be significantly reduced with a combination of RMP and gas injection. Our results indicate that ELM *mitigation* at higher density and gas puffing rates may be more readily-attained than complete ELM *suppression*.

## REFERENCES


[1] G. Federici, *et al.*, Plasma Phys. Control. Fusion **45**, 1523 (2003).

[2] T.E. Evans, *et al.,* Phys. Rev. Lett. **92**, 235003 (2004).

[3] Y. Liang, *et al.*, Plasma Phys. Control. Fusion **49**, B581 (2007).

[4] T.E. Evans, *et al.*, Nucl. Fusion **48**, 024002 (2008).

[5] F. Najmabadi, *et al.*, Fusion Eng. and Design **38**, 3 (1997).

[6] J. Rapp, *et al.,* Nucl. Fusion **44**, 312 (2004).

[7] A. Kallenbach, *et al.*, J. Nucl. Mater. **337-339**, 732 (2005).

[8] T.W. Petrie, *et al.,* J. Nucl. Mater. **363-365**, 416 (2007).

[9] T.W. Petrie, *et al.,* Nucl. Fusion **48**, 045010 (2008).

[10] T.E. Evans, *et al.,* Phys. Plasmas **13**, 056121 (2006).

[11] D.M. Thomas, *et al.,* Plasma Phys. Control. Fusion **48**, A183 (2006).

[12] P.B. Snyder, H.R. Wilson, *et al.,* Phys. Plasmas **9**, 2037 (2002).

[13] M.E. Fenstermacher, *et al.,* J. Nucl. Mater. **363-365**, 476 (2007).

[14] T.D. Rognlien, *et al.*, J. Nucl. Mater. **196-198**, 347 (1992).

[15] T.W. Petrie, *et al.*, Nucl. Fusion **49**, 065013 (2009).

## ACKNOWLEDGMENT

This work was supported by the U.S. Department of Energy under DE-FC02-04ER54698, DE-AC52-07NA27344, DE-FG02-07ER54917, DE-AC05-06OR23100, DE-AC04-94AL85000, and DE-FG02-05ER54809.